# A Histogram-Difference Method (HDM) for Neutron/Gamma Discrimination Using Liquid and Plastic Scintillators

Robert M. French, *Member, IEEE* Mathieu Thevenin, *Senior Member, IEEE*, Matthieu Hamel, Eva Montbarbon

***Abstract*—This paper introduces a novel and extremely simple – and therefore, easily implemented in a Field-Programmable Gate Array (FPGA) – method of neutron/gamma pulse discrimination called the Histogram-Difference Method (HDM). Crucially, this method relies on the use of a "reference set" of $\gamma$-only pulses from $^{22}$Na, $^{137}$Cs and $^{60}$Co sources and on features extracted from the pulses. The pulses from this reference set are compared to a set of an identical number of n+$\gamma$ pulses from a $^{252}$Cf source. Not only can HDM determine the presence of neutrons in the $^{252}$Cf source, but it can also estimate the approximate percentage of neutron pulses from that source. The results reported in this paper are based on data from different radioactive sources and a standard scintillator for this type of research – namely, BC-501A. These results were confirmed using three other scintillators, one made in-house, and two others that are commercially available, EJ-299-33 and EJ-200. Pulses were encoded using Q-values, which are features extracted from the pulses, i.e., ($Q_{total}$, $Q_{tail}$) pairs in $\mathbb{R}^2$. As a control, we also encoded pulses as the Root-Mean-Square (RMS) distances from the average pulse of all known $\gamma$-only pulses and ran HDM using these pulse representations. The results are very similar to those obtained using a Q-value encoding of the pulses.**

***Index Terms*—neutron-gamma discrimination, plastic scintillators, Qtail, Qtotal**

## I. Introduction

DESPITE strict international regulations and the Non-Proliferation Treaty (NPT), dissident countries may attempt to develop weapons using fissile material. The main hurdle confronting these countries is the lack of availability of fissile substances, since their trade is prohibited by the NPT. They must, therefore, obtain these materials from illegal sources. Public transportation infrastructures, such as, railroads, highways, and harbors can be used to transit this material since most countries do not police these transit infrastructures closely. Therefore, detecting fissile material in harbors, airports or anywhere that is accessible to vehicular traffic, is essential if we are to limit this illegal trade, in order to ensure the respect of the NPT and to protect the population from the risks associated with the dissemination of these materials. Some countries, such as the United States, have begun setting up border checks that are specifically designed to detect these threats. They have installed large numbers of neutron-detection portals that are specifically designed to detect radiological threats. Fission chambers are very good neutron detectors, but they contain fissile materials and cannot be used outside of controlled areas, such as airports or harbors. Today the most common means of neutron detection involves the use of Helium-3 ($^3$He) gas [1]. $^3$He has a high thermal neutron absorption capacity that allows easy neutron/gamma (n/$\gamma$) discrimination by means of a very simple and robust signal filtering and its intrinsic insensitivity to $\gamma$-rays. However, $^3$He is a rare gas obtained only from tritium stocks, traditionally used for hydrogen bombs. As the potential for fissile material trafficking has increased, more neutron-detection portals have been needed and in the last decade, this has led to a global shortage of $^3$He [2], a situation that urgently requires the development of alternative neutron-detection technologies.

However, unlike neutron detection by $^3$He, other alternatives are sensitive to $\gamma$-rays, and, unfortunately, neutron emission produces significant levels of $\gamma$-ray emission which masks neutron flux. In addition, many perfectly legitimate materials (e.g., $^{40}$K in bananas) also emit $\gamma$-rays. In short, the development of novel n/$\gamma$ discrimination techniques [3] is crucial to ensure the future security of countries.

Currently two technologies hold considerable promise for $^3$He replacement. The first is based on the use of $^6$Li/ZnS(Ag) screens coupled to wavelength-shifting fibers for thermal neutron detection [4]. In this technique [5] a simple Pulse Shape Discrimination (PSD) is performed to eliminate background $\gamma$ radiation. This technique has the advantage of allowing straightforward replacement of the $^3$He tubes. However, due to its ability to detect only thermal neutrons, this technique provides little or no information about neutron energy levels. Nonetheless, commercial applications of this technology are beginning to appear.

The second technology relies on organic and plastic scintillators [6], which are able to detect thermal neutrons, fast neutrons, and gamma rays. In addition to having a low manufacturing cost, these scintillators require little subsequent maintenance. Plastic scintillator technology, once it has been scaled up to industrial production, could well be the basis of the next generation of neutron-detection portals. In terms of their intrinsic efficiency and their ability to meet American National Standards Institute (ANSI) requirements, plastic scintillators are almost as effective as $^3$He detectors [3]. As for liquid scintillators, their performance can sometimes even exceed that of $^3$He.

The main problem, however, is that scintillators are sensitive

Robert M. French is a Research Director with French National Center for Scientific Research (CNRS), LEAD-CNRS UMR 5022, UBFC, Dijon.

Mathieu Thevenin, Matthieu Hamel and Eva Montbarbon are with the CEA, LIST, the French Atomic Energy Commission.

to both neutron and $\gamma$ radiation, which means that they are not amenable to easy n/$\gamma$ discrimination using the standard signal-processing approaches commonly used in nuclear science, such as simple thresholding or spectroscopy. Moreover, chemical modifications of the plastic scintillators can sometimes lead to unexpected deformations or ageing of the material, as occurred, for instance, with the EJ-299-33 commercial scintillator [6].

Current signal-processing algorithms for n/$\gamma$ discrimination in plastic scintillators require a deep understanding of the photophysical processes involved in the interactions within the scintillator. Gamma radiation and neutrons are responsible for producing singlet and triplet states, respectively yielding prompt and delayed luminescence. The delayed luminescence induced by neutrons can be observed in plastic scintillators specifically designed to enhance the phenomenon. However, to date, digital signal-processing approaches to optimize n/$\gamma$ discrimination by means of plastic scintillators have not been fully explored. Traditional approaches are based on PSD [7], [8], [9], [10], [11] or Time Of Flight (TOF) [12] differences between two separated scintillators. More recent strategies, (e.g., [13], [14], [15], [16], [17]) propose applying digital signal-processing techniques applied to PSD. Since all components of a pulse-acquisition system play a role in determining the performance of the system, the choice of both the detector and the PhotoMultiplier Tube (PMT) impacts performance [18], [19]. Arguably, the primary difficulty of signal-processing methods resides in the impossibility of acquiring neutron-only pulses with plastic or liquid scintillators. Even if the scintillator is completely shielded from $\gamma$ rays, neutrons will interact with it or its environment, thereby producing significant numbers of gamma pulses that interfere with the neutron measurement. In contrast to the difficulty, even impossibility, of obtaining a dataset consisting only of neutron pulses, obtaining a dataset of $\gamma$-only pulses is straightforward, a fact that is crucial to the the algorithm presented in this paper.

Our task is to determine the approximate percentage of neutron pulses produced by a n+$\gamma$ source using a plastic or liquid scintillator. We will present a generic approach that can be used with various types of detectors, various types of PMT, even a Silicon PhotoMultiplier (SiPM), provided that the pulses obtained from the neutrons differ, however slightly, from those obtained from $\gamma$-rays. We will illustrate the Histogram-Difference Method (HDM) algorithm with a BC-501A scintillator, but it can be applied to any pulse-acquisition system.

The remainder of this paper is organized as follows. Section II presents a method of pre-processing and normalizing pulses from $\gamma$-only emitters ($^{22}$Na, $^{137}$Cs, and $^{60}$Co) and from a n+$\gamma$-emitter ($^{252}$Cf). We then describe in section III the underlying theory of the HDM algorithm that allows us to determine whether or not a given material is neutron-emitting and, if so, to quantify the minimum percentage of neutron pulses observed using traditional plastic or liquid scintillators. Section IV shows how pulses can be represented for HDM. It also discusses how we determine the parameter values of the HDM algorithm. Finally, we check our results by using a different encoding of the pulses. Section V presents the results obtained using a standard liquid scintillator (BC-501A), along with three other plastic scintillators. This section also presents the impact of the number of pulses from a n+$\gamma$ source on the quality of n/$\gamma$ discrimination.

## II. Signal Preprocessing

PSD methods rely on the fact that neutron and $\gamma$ pulses are responsible for producing singlet and triplet states that result in delayed and prompt luminescence, respectively. Delayed luminescence induced by neutrons can be observed in the signal produced by scintillators designed for this purpose. However, discriminating neutron and $\gamma$ pulses remains very difficult. The reasons for this can be seen in Figure 1. The top panel (1a) of this figure shows in red an "average" $\gamma$ pulse produced by averaging 15,000 (peak-aligned and normalized) $\gamma$ pulses from three different $\gamma$-only sources ($^{22}$Na, $^{137}$Cs and $^{60}$Co), denoted in the text as $S_\gamma$. On the same graph is superimposed an average pulse (blue) from 15,000 (peak-aligned and normalized) pulses from a $^{252}$Cf source (i.e., n+$\gamma$), denoted in the text as $S_{n+\gamma}$. The two average pulses are almost identical. It is important to note that we cannot directly obtain n-only pulses from a $S_{n+\gamma}$source (or any source, for that matter). There will necessarily be a mixture of neutron and $\gamma$ pulses. Our task is to determine the percentage of neutron pulses from the $^{252}$Cf (or any other $S_{n+\gamma}$) source. What makes this task particularly challenging is that, in addition to the fact that the average pulses produced by the $\gamma$-only and the n+$\gamma$ sources are extremely similar, there is significant variability of the n+$\gamma$ pulses (Figure 1b) and the $\gamma$-only pulses (Figure 1c).

### A. Pulse Capture

Pulse acquisition was carried out as illustrated in Figure 2 for both a n+$\gamma$ source and a $\gamma$-only source. The scintillator used for our experiments was the commercially available liquid scintillator BC-501A placed in a sealed white-painted cell (2"×2"). The scintillator was optically coupled to a Hamamatsu R7724-100 PMT equipped with a Super Bialkali photocathode. The anode fed a CAEN DT5743 digitizer. This DAQ system has a 500 MHz bandwith so that Shannon′s theorem is valid for the scintillator rise-time. Its resolution is 12 bits and we fixed the sampling rate at 800 MSamples/s. Three $\gamma$-only sources were used during our experiments: $^{22}$Na (2.86 MBq), $^{137}$Cs (530 kBq), and $^{60}$Co (150 kBq). The n+$\gamma$ source is $^{252}$Cf (540 kBq). A similar procedure was used for a number of other scintillators; we simply used a faster PMT for the EJ-299-33 and the EJ-200 plastic scintillators.

### B. Pulse Pre-processing

For PSD to work correctly, acquired pulses must be normalized and peak-aligned, so as to be mutually comparable. This section describes the normalization and peak-alignment procedures for pulses obtained from the BC-501A scintillator, but they can be used with any other detector. Parameters must be adapted to the pulse length. Pulses are first detected by a threshold-based trigger and

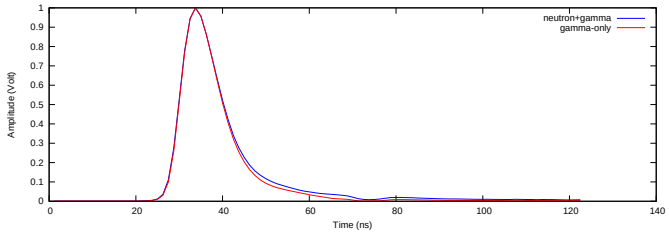


(a)

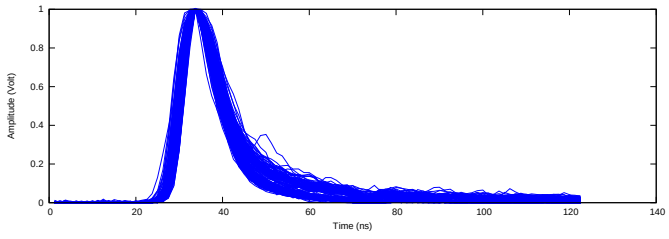


(b)

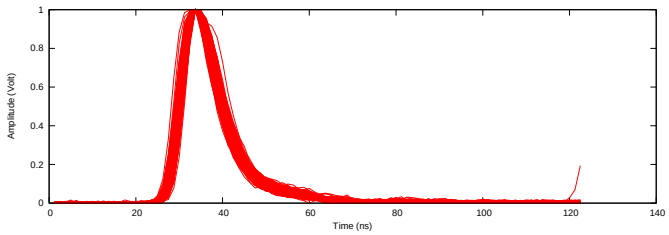


(c)

Fig. 1: Superimposed pulses after acquisition for a) averaged pulses from n+$\gamma$ (blue) pulses and for $\gamma$-only (red) pulses; b) the variability of 250 n+$\gamma$-pulses from $S_{n+\gamma}$ ($^{252}$Cf) and c) the variability of 250 $\gamma$-only pulses from $S_{\gamma}$.

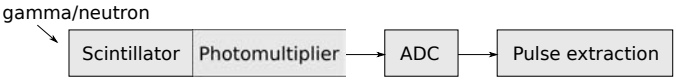


Fig. 2: Acquisition layout.

the baseline is adjusted to define a common zero-level. We need a common relative time reference and chose to use the peak amplitude of the pulses as this reference. We, therefore, align all pulses so that their peak amplitude falls at $t_{max} = 0$ ns. Figure 3 shows 150 superimposed raw $\gamma$ pulses.

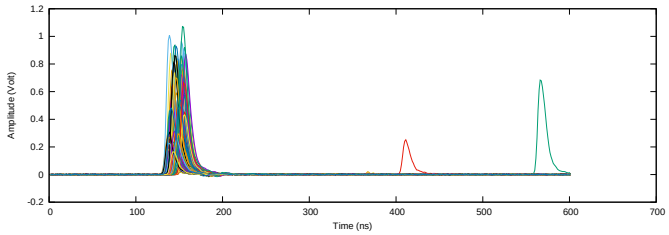


Fig. 3: Superimposed $\gamma$ pulses prior to peak-alignment at $t_{max} = 0$ ns and normalization. Note the spurious pulses to the right also have to be eliminated. Only pulses with amplitude above 0.10 V were included.

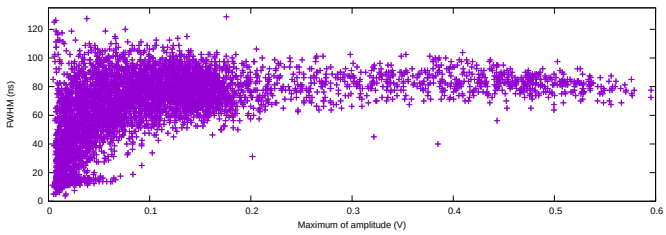


Fig. 4: Pulses' FWHM versus maximum of amplitude for an in-house, laboratory-grade plastic scintillator.

The maximum amplitude of these pulses can be seen to vary significantly. For this reason, we normalize all pulses with respect to their peak amplitude. In addition, the width of all pulses must be of the same order of magnitude, regardless of their amplitude. This is the case for inorganic scintillators, including BC-501A. However, for organic scintillators, Birks law must be applied [20]. For low energies, the energy loss in the scintillator may have a significant effect on pulse width. We determine the maximum amplitude corresponding to the energy level above which the energy loss due to the scintillator has essentially no impact on pulse width. This can be done by plotting the Full Width at Half Maximum (FWHM) versus the maximum amplitude corresponding to the energy deposited in the scintillator. As can be seen in Figure 4, above a certain peak amplitude (when energy loss is relatively low compared to the total energy of the pulse), the FWHM for all pulses is of the same order of magnitude. In other words, to make the pulses comparable, we must select pulses with comparable FWHM values. To do this, we set the pulse detection threshold to 0.10 V and filtered all pulses to ensure that the FWHM fell within a predefined range – in this case from 60 to 100 ns. (Note: Instead of preselecting acceptable pulses for normalization to enable a fair comparison between them, another approach would have been to correct the energy loss induced in the plastic scintillator by applying an inverse transfer function to the detector.)

After the above pre-processing to ensure that the FWHM for all pulses is of the same order of magnitude, the pulses are then normalized with respect to their maximum amplitude and peak-aligned. Figures 1b and 1c show sets of 250 n+$\gamma$ pulses and 250 $\gamma$-only pulses, respectively, that have been FWHM-filtered, peak-aligned and normalized. Figures 5 and 6 show a three-pulse set composed of 481 time-samples before and after FWHM filtering, peak-alignment and normalization. After maximum-amplitude normalization and peak-alignment, all pulses are comparable, a precondition to all PSD approaches.

## III. The Histogram-Difference Method principle

HDM is based on two key assumptions: a) that the distribution of the features of representations of pulses from any $\gamma$-only source will be very similar and b) the difference between the $\gamma$-pulse feature distribution and the (n+$\gamma$)-pulse feature distribution for an identical number of $\gamma$-only and (n+$\gamma$) pulses will allow us to determine a lower bound on the percentage of

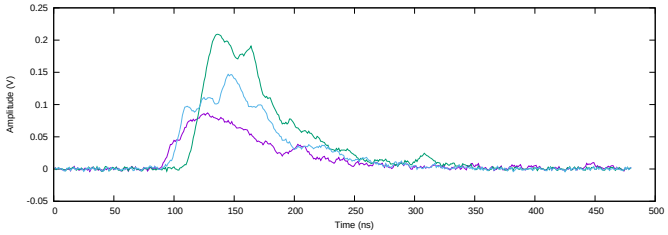


Fig. 5: A 3-pulse set composed of 481 samples before FWHM filtering, peak-alignment and normalization.

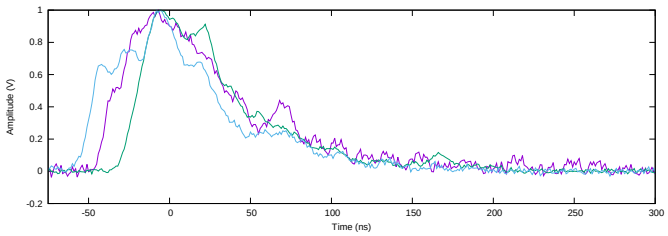


Fig. 6: A 3-pulse set composed of 481 samples after FWHM filtering, peak-alignment and normalization.

neutron pulses in the set of (n+$\gamma$) pulses. Crucially, the method relies on the use of a set of pulses from an independent $\gamma$-only source that serves as a "reference" set to which any source containing a mixture of n and $\gamma$ pulses can be compared.

Let us start with a "toy" example to illustrate the principles of HDM. For didactic purposes, we suppose that each pulse can be represented by a single integer from 1 to 5. We will call this value the Representation-value, or R-value, that characterizes the pulse. Suppose further that there is a set of exactly 10 $\gamma$ pulses comprising the "$\gamma$-pulse reference set" and a set of exactly 10 n+$\gamma$ pulses for which we wish to determine the percentage of neutron pulses. We start by producing a 5-bin histogram for the R-values that characterize our 10 $\gamma$ pulses. This histogram is shown in Figure 7a. We make the key assumption that *any* set of 10 $\gamma$-only pulses will produce exactly this histogram.

Now we consider the set of R-values for the 10 pulses comprising the n+$\gamma$ pulses. We bin these values as we did for the R-values from the $\gamma$ pulses. This produces the histogram shown in Figure 7b. If this second set of pulses had contained only $\gamma$ pulses, our assumption is that it would have produced exactly the same histogram as the one in Figure 7a. But this was not the case. There is now one less R-value in bin 5 and one more in bin 2. Since we have exactly 10 $\gamma$ and 10 (n+$\gamma$) pulses, this change can only be due to a single n pulse. Because we have one less R-value in bin 5 and one additional R-value in bin 2, the absolute difference between the $\gamma$-only and the (n+$\gamma$) histograms is 2. But these 2 changes were both caused by one less R-value in bin 5, compensated for by one more R-value in bin 2, as illustrated in Figure 7c. In other words, the presence of an extra (neutron-pulse) R-value somewhere means that there is necessarily one fewer gamma-pulse R-value somewhere else (unless the neutron R-value and the gamma R-value are exactly the same). This means we must divide the number of changes between the $\gamma$-only histogram and the n+$\gamma$ histogram by 2. Thus, there is at least one neutron pulse in our set of 10 n+$\gamma$ pulses and we can conclude that the percentage of neutrons among the n+$\gamma$ pulses is at least 10%.

A further advantage of this method is that, even if a number of neutron pulses have R-values that are identical to those of pure-$\gamma$ pulses, it is likely that the overall R-value distribution for n+$\gamma$ will be different than the R-value distribution for the $\gamma$-only pulses. The histogram-difference method requires there to be *exactly* the same number of pulses from our $\gamma$-only source and from the n+$\gamma$ source. The principles of this toy example using R-values and 2D histograms apply *mutatis mutandis* to real $\gamma$ pulses and n+$\gamma$ pulses. In the "toy" example, the R-values are real values (i.e. one-dimensional vectors), which produces a 2D histogram. However, the approach we are proposing can be used with N-dimensional vectors of pulse-features, which produce a N+1 dimensional histogram.

## IV. Pulse Representation and Algorithm Parameters

This section presents HDM using pulses acquired from BC-501A and different sources of $\gamma$-rays and neutrons. It discusses in detail how pulse features are extracted.

### A. Feature extraction

Once pulse pre-processing is completed, each normalized, peak-aligned pulse is then represented by a single real value (D-values) or by a pair of real values (i.e. features) extracted from the pulses (Q-values). D-values and Q-values are discussed in detail below. Pulse representation is not limited to

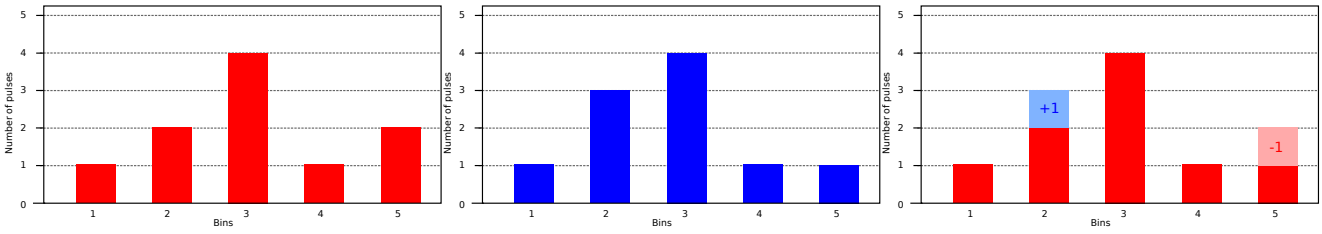


(a) (b) (c)

Fig. 7: A toy example illustrating the Histogram-Difference Method (HDM) using bins of R-values representing the pulses from a) $S_\gamma$, b) $S_{n+\gamma}$and c) how to calculate difference between $\gamma$-only and n+$\gamma$ pulses.

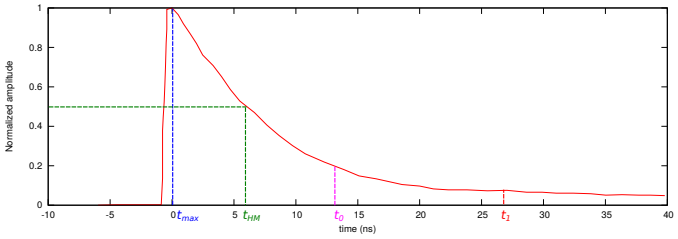


Fig. 8: When representing each pulse, we consider only energy values after the peak value. We define two constants, $t_0$ and $t_1$, which are linear functions of $d_{HM}$, the distance between the t-value of the maximum-amplitude peak of the pulse ($t_{max}$) and the t-value, $t_{HM}$, corresponding to the Half-Maximum height of the pulse curve.

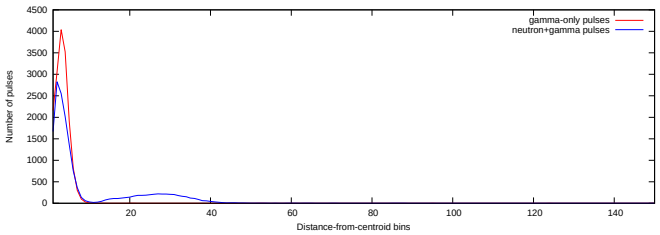


Fig. 9: Histograms based on RMS-distances from the centroid, C$\gamma$ of all known $\gamma$-only pulses to the reference set of $\gamma$-only pulses (red) and from C to the same number of pulses from the $^{252}$Cf source (blue).

these two types of representation, but as we wish to show that HDM is not representation-bound, we test it with these two different, independent pulse representations. Both D-values and Q-values rely on two values, which we will call $t_0$ and $t_1$. These two values are shown in red in Figure 8.

All pulses are rectified, FWHM-filtered, normalized and peak-aligned at $t_{max}$, consequently, we can consider $t_{max}$ as our time reference. We remove all energy values of the pulse before $t_{max}$. We define $d_{HM}$ as the time required for the pulse height to decrease to half of its maximum value (peak value) starting from the peak value. This value can be expressed by $d_{HM} = t_{HM} - t_{max}$. We then define $t_0$ and $t_1$ by equations 1 and 2 where $\alpha$ and $\beta$ are user-defined constants.

$$t_0 = t_{max} + \alpha \times d_{HM} = \alpha \times d_{HM} \quad (1)$$

$$t_1 = t_{max} + \beta \times d_{HM} = \beta \times d_{HM} \quad (2)$$

The reason we define $t_0$ and $t_1$ with respect to $d_{HM}$ is because the width of pulses can vary considerably depending on the type of scintillator used. For the BC-501A liquid scintillator, the reference scintillator for this paper, $d_{HM}$ is approximately 7.50 ns wide. For other scintillators (e.g., the plastic scintillator, EJ-299-33), the average $d_{HM}$ is more than twice as wide as $d_{HM}$ for BC-501A, approximately, 13.25 ns. Defining $t_0$ and $t_1$ in terms of $d_{HM}$, normalizes how we represent pulses from different scintillators, thus allowing us to compare the performance of various scintillators.

Selecting the values of $t_0$ and $t_1$ is not entirely straightforward. It turns out that in order to best discriminate pulses from a neutron source ($S_{n+\gamma}$) from those emitted by a $\gamma$-only source ($S_\gamma$), the zone of maximal-discrimination information lies in the mid-range of the tails of the pulses. For example, when we average all of the pulses in $S_\gamma$ and those in $S_{n+\gamma}$ we find that there is essentially no difference between the two average pulses far out on their tails (Figure 1a). For this reason it is important to select values of $t_0$ and $t_1$ that a) allow the best discrimination of $S_\gamma$ and $S_{n+\gamma}$ while, at the same time, b) ensure that the observed discrimination is not simply produced by noise in the respective pulses. However, before we can specify how the values of $t_0$ and $t_1$ are determined, we need to discuss the histogram-difference algorithm.

### B. D-Values

The first way of representing pulses is by means of what we call "D-values". We start with a set of pulses from a $\gamma$-only source ($S_\gamma$). $S_\gamma$ is what we call the $\gamma$-only reference set of pulses. For each pulse in this reference set we create a vector, $E$, consisting of its energy values that lie between $t_0$ and $t_1$. We then calculate the average energy vector for all pulses in $S_\gamma$ and call this vector $C_\gamma$ (for "centroid"). Then for each pulse, $p_k$, in $S_\gamma$ we compute the Root-Mean-Square (RMS) distance, $d$, from its $t_0$-to-$t_1$ energy vector, $E_k$, to $C_\gamma$ (i.e., $D_k = d(C_\gamma, E_k), \forall p_k \in S_\gamma$). We do the same for the set of pulses, $S_{n+\gamma}$, that we wish to compare to $S_\gamma$. So, for each pulse, $p_i$, in $S_{n+\gamma}$, we determine its $t_0$-to-$t_1$ energy vector, $E_i$, and calculate the RMS distance, $d$, from $E_i$ to $C_\gamma$, (i.e., $D_i = d(C_\gamma, E_i), \forall p_i \in S_{n+\gamma}$). In short, each pulse, whether in $S_\gamma$ or in $S_{n+\gamma}$, is characterized by its RMS distance from the $\gamma$-only centroid pulse, $C_\gamma$, which corresponds to its D-value.

We use as our $\gamma$-only reference set of pulses, $S_\gamma$, the set consisting of equal numbers of $^{22}$Na, $^{137}$Cs, and $^{60}$Co pulses. There are a total of $N = 16,000$ pulses in this combined set. We calculate a set of D-values for all pulses in this set. We do the same for the $16,000$ pulses in the n+$\gamma$ set, $S_{n+\gamma}$ (i.e., pulses from $^{252}$Cf).

Since each pulse is represented by a single number (i.e., its RMS distance from C$\gamma$), we require a 2D histogram in which the abscissa represents the binned distances (250 bins) from C$\gamma$ and the ordinate is the number of pulses in each of these bins. The histograms for all $\gamma$-only (red) and n+$\gamma$ pulses (blue) are shown in Figure 9. They clearly show the presence of neutrons in $^{252}$Cf. As in the toy example, based on the difference between these two D-value histograms we obtain an approximate lower bound on the percentage of neutron pulses from the $^{252}$Cf source of $27.2\%$. Using other techniques, this value has been reported elsewhere in the literature to be between $25\%$ and $30\%$ [21], [22], [23].

### C. Q-values

There are, of course, many other ways in which pulses could be represented. One widely used representation associates a pair of real-number values, ($Q_{total}$, $Q_{tail}$), with each pulse [24], [25], [26]. We refer to this pair of values for a given pulse as its Q-value. This is a standard means of representing pulses and derives from the well-known fact that neutron and

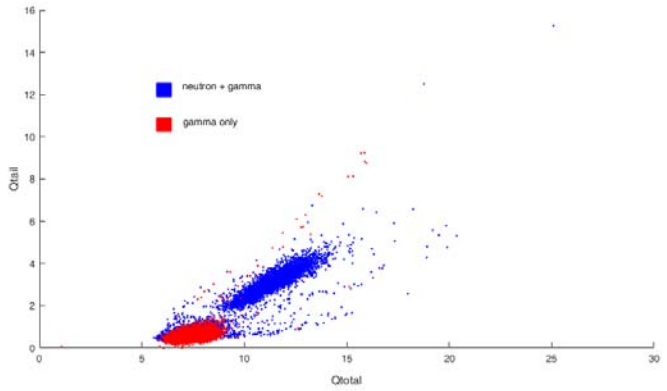


Fig. 10: Q-value scatterplot for a sample of $^{22}$Na+$^{137}$Cs+$^{60}$Co (red, $\gamma$-only) and $^{252}$Cf (blue, n+$\gamma$).

gamma pulses differ most after their peak energy. Standard PSD-based n/$\gamma$ discrimination approaches assume that pulses obtained from gamma-ray interactions are very similar to those produced by neutrons, except that the former have somewhat less energy in the tail than the latter (Figure 1a). The components of the Q-value pair, $Q_{total}$ and $Q_{tail}$, are defined in Equations 3 and 4.

$$Q_{tail} = \int_{t_0}^{t_1} f(t)dt \tag{3}$$

$$Q_{tot} = \int_{t_{max}}^{t_1} f(t)dt \tag{4}$$

where $t_{max}$, $t_0$, and $t_1$ are as shown in Figure 8.

*1) Scatterplots vs. histograms:* Scatterplots of Q-values for pulses obtained from $\gamma$-only and n+$\gamma$ sources are generally represented as in Figure 10. However, this 2D scatterplot contains no information about the number of similar Q-values. We, therefore, divided the 2D scatterplot into a $300 \times 150$ grid and produced a 3D histogram of the Q-values (in $\mathbf{R}^2$) that also indicates the number of similar Q-values in each cell of the grid[1]. In this manner we produce a 3D "reference" histogram for the $\gamma$-only pulses and another 3D histogram for the n+$\gamma$ pulses. In order to better visualize these histograms, we use a contour plot with 150 contour levels, as shown in Figure 11.

*2) The "$\gamma$-only reference" histogram:* Key to HDM is the "$\gamma$-only reference histogram" which is a 3D histogram representing the distribution of Q-values for pulses from a $\gamma$-only reference source. Histograms from various $\gamma$-only sources vary slightly, notably in their variance. To ensure that our results were not influenced by these variations, we combined pulses from three separate $\gamma$-only sources – namely, $^{22}$Na, $^{137}$Cs and $^{60}$Co. An underlying assumption of HDM is that all $\gamma$-only pulse histograms, regardless of the features used to represent the pulses, are essentially identical. Once we have a $\gamma$-only reference histogram, $H_\gamma$, derived from $N$ $\gamma$-pulses we compare it to the histogram, $H_{n+\gamma}$, produced by exactly $N$ pulses from the n+$\gamma$ source. In other words, we do not attempt to directly discriminate neutron and gamma pulses from a single n+$\gamma$ source, as is done by most current n/$\gamma$ discrimination techniques. Rather, we begin by producing a "$\gamma$-pulse reference histogram" from a set of *N* (in our case, 16,000) known $\gamma$-only pulses. We build this histogram by counting the number of pulse Q-values (i.e., the ($Q_{total}$, $Q_{tail}$) pair for each pulse) that fall into each cell of a $300 \times 150$ grid. This provides an accurate Q-value distribution for known $\gamma$-only pulses. We then compare this reference histogram, $H_\gamma$, to the corresponding Q-value histogram, $H_{n+\gamma}$, produced by exactly *N* pulses obtained from the n+$\gamma$ source. The difference between these two histograms allows us to approximate the percentage of neutron pulses from the n+$\gamma$ source.

*3) HDM using neutron and $\gamma$ Q-values:* In a real situation, we compare the $\gamma$-only Q-value reference histogram derived from 16,000 pulses from the $\gamma$-only source (identical numbers of pulses from $^{22}$Na, $^{137}$Cs and $^{60}$Co) with the histogram for 16,000 pulses from an unknown n+$\gamma$ source. Since there are exactly the same number of pulses from the $\gamma$-only reference

[1]The size of the grid is a parameter of the algorithm

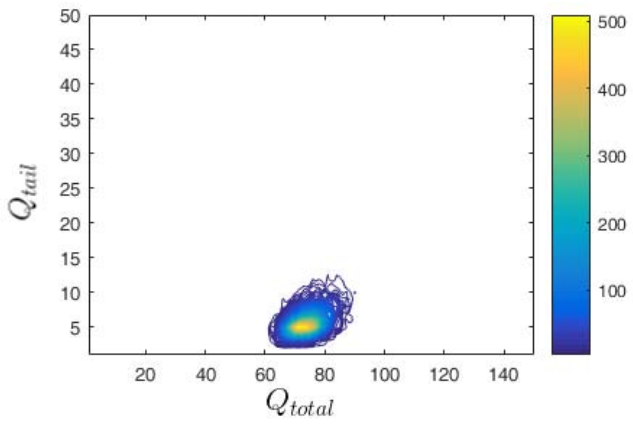


(a)

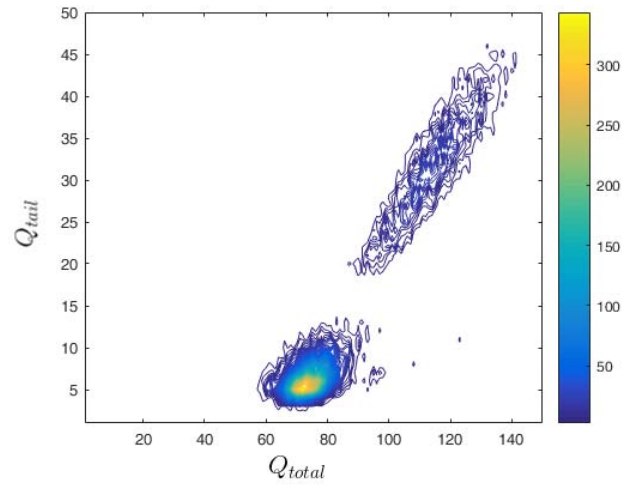


(b)

Fig. 11: Histogram contour plots for a) 16,000 reference pulses from a combined $\gamma$-only source ($^{22}$Na+$^{137}$Cs+$^{60}$Co); b) 16,000 n+$\gamma$ pulses obtained from a $^{252}$Cf source. The original $300 \times 150$ grid has been truncated to $150 \times 50$ because only a very small number of ($Q_{total}$, $Q_{tail}$) values fell outside of the truncated zone. 150 contour levels were used.

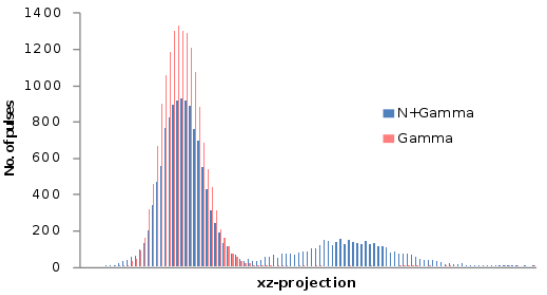


Fig. 12: A summed projection onto the yz-plane of the 3D Q-value histogram of $16,000$ $\gamma$-only pulses (red) and $16,000$ n+$\gamma$ pulses (blue). This graph illustrates the principle of the HDM: the differences with respect to the $\gamma$-only reference histogram (red) are due to the presence of neutrons. The difference in the two summed projections allows us to determine the approximate percentage of neutrons in the n+$\gamma$ set.

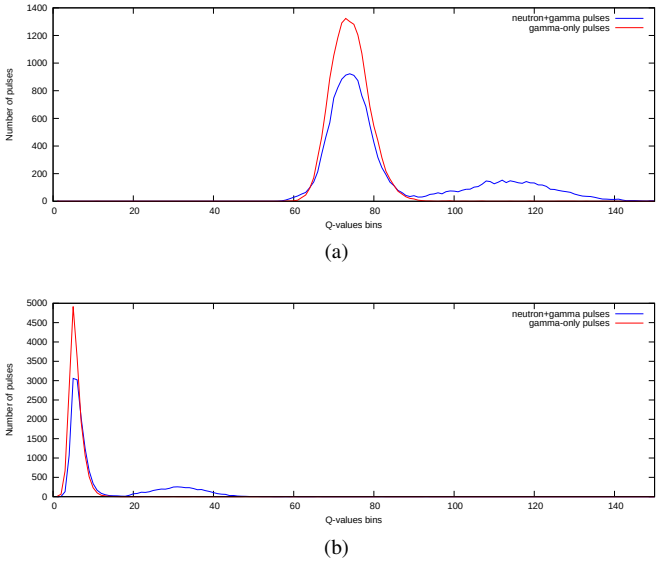


Fig. 13: (a) xz summed projections of the $\gamma$-only (red) and the n+$\gamma$ (blue) histograms for $16,000$ pulses. (b) yz summed projection for the same histogram as in (a).

source and the n+$\gamma$ source, any difference in the 3D Q-value histograms for the $\gamma$-only source and the n+$\gamma$ source will necessarily be due to neutrons. Thus, as in the toy example, any decrease in one of the bins of the $\gamma$-only histogram must be compensated for by a corresponding increase in a bin somewhere else in the histogram. It is the difference in these two histograms that allows us a) to say that there are neutron pulses in the n+$\gamma$ source and b) to approximate their percentage. This is clearly indicated in Figure 12.

One way to illustrate the differences in the $\gamma$-only and the n+$\gamma$ 3D histograms is by comparing their "summed projections". A summed projection is much like a standard projection except that, instead of projecting a "shadow" of the 3D histogram onto the xz and yz planes, we sum all of the columns of the 3D histogram along the projection axis and graph this sum on the projection plane. The summed projections of the $\gamma$-only and the n+$\gamma$ 3D Q-value histogram contour-plots in Figure 11 (smoothed with a Gaussian filter with $\sigma = 0.5$) are shown in Figures 13a and 13b. We can clearly see the differences between the summed projections for the $\gamma$-only reference histogram (red) and the n+$\gamma$ histogram (blue), indicating the presence of neutrons in the $^{252}$Cf source.

### D. Determining the values of $t_0$ and $t_1$

We are now in a position to discuss how we determined the values of $t_0$ and $t_1$. Recall that $t_0$ was given by Equation 1 and $t_1$ by Equation 2 with $\alpha$ and $\beta$ parameters to be determined. What we want are values for $\alpha$ and $\beta$, such that: i) the overall difference between the values the of $\gamma$-only pulses and the n+$\gamma$ pulses between $t_0$ and $t_1$ is as large as possible, thereby ensuring good discrimination and ii) $t_0$ and $t_1$ are not so large that any neutron/gamma differences observed in the two sets of pulses between these two values are due to random fluctuations in the tails of the pulses. To determine these values, we examined a range of $\alpha$ values from $0.5$ to $12$ and a range of $\beta$ values from $4$ to $100$.

We then picked values for $\alpha = 4$ and $\beta = 20$ (the white dots in Figures 14a and 14b) that gave both a high value of discrimination (Figure 14a), while at the same time, were in an area of low estimated fractions of neutron pulses due to random fluctuations in the tails of the pulses. These two graphs show that we could have picked other values for $\alpha$ and $\beta$, for example $\alpha = 4$ and $\beta = 8$, in order to determine $t_0$ and $t_1$. These values of $\alpha$ and $\beta$ would also have produced values of $t_0$ and $t_1$, that would have allowed HDM to produce good results, showing that $^{252}Cf$ produced approximately $30$ $\%$ neutron pulses.

## V. Results and Discussion

This section presents the results of HDM using different scintillators. In addition, it shows the impact of reduced numbers of n+$\gamma$ pulses on the quality of the results.

### A. Results using different scintillators

We tested HDM on a number of different liquid and plastic scintillators. E32 refers to a laboratory-grade plastic scintillator developed in-house [11]. BC-501A is the standard, liquid scintillator used for testing various methods of n/$\gamma$ pulse discrimination. EJ-299-33 and EJ-200 are two other, standard, commercially available scintillators. For each of these scintillators we measured the percentage of neutrons in a $^{252}$Cf source. HDM allows us to say that the $^{252}$Cf source does, indeed, emit neutrons and that approximately $29.9\%$ of the pulses are neutron pulses which corresponds to the quantity expected. This figure corresponds closely to what we found using D-value representations for the pulses (see Section IV-B), but also to values found by other techniques [21], [22], [23].

We also tested our $\gamma$-only sources (mixture of $^{22}$Na+$^{137}$Cs+$^{60}$Co) by splitting the original set of $16,000$ pulses into two random sets of $8,000$ pulses.

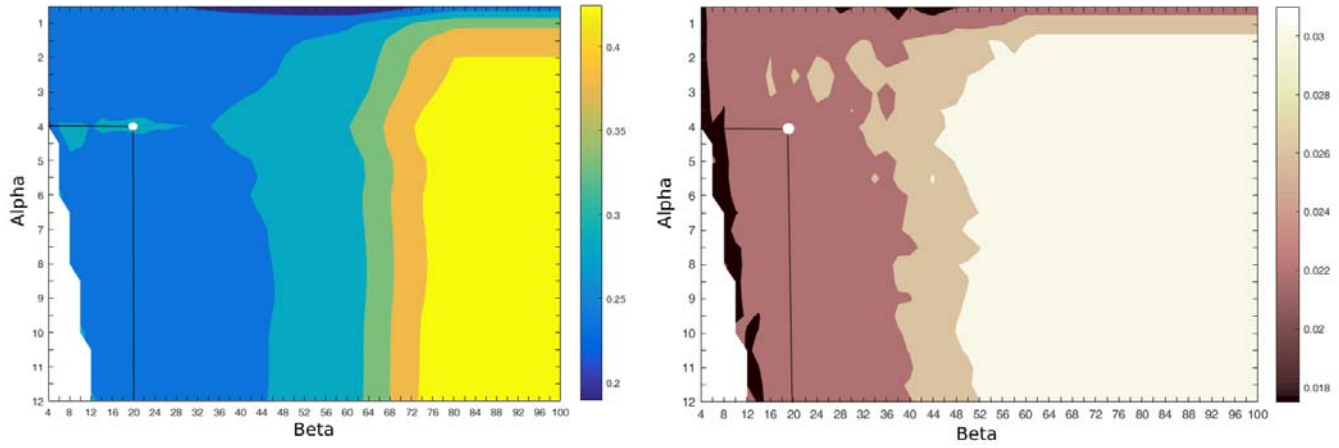


(a) (b)

Fig. 14: a) Estimated fraction of neutron pulses in $S_{n+\gamma}$ depending on the values of $\alpha$ and $\beta$; the determination of the best values for $\alpha$ and $\beta$ is given by the white dot; b) (false) estimated fraction of neutron pulses in the $\gamma$-only reference set (the true fraction is, of course, 0% since all pulses were from a $\gamma$-only source).

TABLE I: Comparison of HDM for several types of liquid and plastic scintillators.

| Scintillator | Neutron estimate (%) | |
|---|---|---|
| | $^{252}$Cf | $\gamma$-only sources |
| BC-501-A | 29.9 | 4.0 |
| E32 | 26.0 | 4.0 |
| EJ-299-33 | 26.3 | 4.0 |
| EJ-200 | 23.2 | 4.0 |

We then compared the first set of pulses against the second to determine the percentage of neutrons that the HDM (incorrectly) estimated that the first set of pulses was emitting. This figure, which we call the n/$\gamma$-discrimination baseline, was $4\%$ as illustrated in Table I.

### *B. Using HDM with small numbers of pulses*

The histogram for the reference set of $\gamma$-only pulses can be scaled to correspond to the number of pulses in the n+$\gamma$ set of pulses. In other words, if $H_\gamma$ is the matrix representing the histogram for N $\gamma$-only pulses, if there are only $n$ pulses from the n+$\gamma$ source, we scale $H_\gamma$ by multiplying it by $n/N$, thereby producing a histogram whose overall number of pulses will be the same as those for $H_{n+\gamma}$. So we have $\hat{H}_\gamma = \frac{n}{N} \cdot H_\gamma$ In this way, even if the values in the scaled histogram are not integers, it will have the same total pulse counts as the histogram of the n+$\gamma$ set of pulses. The advantage of doing this is, of course, that, regardless of the size of the n+$\gamma$ set of pulses, $\hat{H}_\gamma$ will be an accurate, albeit scaled, reflection of the histogram for $16,000$ $\gamma$-only pulses and will be able to be compared appropriately to $H_{n+\gamma}$ .

Because we use a fixed histogram derived from a $16,000$-pulse $\gamma$-only reference-set that we can then scale to correspond to any size of the n+$\gamma$ set of pulses, we need only be concerned with the n+$\gamma$ set of pulses. When the n+$\gamma$ histogram is derived from a small number of pulses (e.g., 100 pulses obtained from a $^{252}$Cf source), a problem arises. The Q-value histogram for the $^{252}$Cf pulses is too sparse to accurately represent the overlap (or in this case, the lack of overlap) between the $\gamma$-only and the n+$\gamma$ histograms. This does not allow us to accurately estimate the number of displaced (i.e., neutron) pulses with respect to the $\gamma$-only histogram. The difference between the two histograms is proportionately larger than it should be (Table II), which means that the estimate of neutron pulses in the set of n+$\gamma$ pulses is too high. With only 100 pulses from $^{252}$Cf, we obtain an estimate of $41.2\%$ neutrons, in other words, an unacceptably high $38\%$ error compared to the value obtained with $16,000$ pulses, namely, $29.9\%$. However, as the number of n+$\gamma$ pulses increases this figure rapidly asymptotes to the value that was obtained with $16,000$ n+$\gamma$ pulses (Figure 15). With $2,000$ pulses, we obtain an estimate of $31.0\%$ neutrons, which is within $4\%$ of the value of $29.9\%$ obtained with eight times as many pulses (i.e., $16,000$ pulses). With $8,000$ pulses n+$\gamma$ pulses the error is below $1\%$.

TABLE II: Number of pulses from the $^{252}$Cf source and neutron estimate with Gaussian smoothing kernel $\sigma = 0.5$

| no. n+$\gamma$ pulses | % neutron estimate |
|---|---|
| 100 | 41.2 |
| 250 | 36.0 |
| 500 | 33.3 |
| 1,000 | 32.4 |
| 2,000 | 31.0 |
| 4,000 | 30.5 |
| 8,000 | 30.1 |
| 16000 | 29.9 |

### *C. Limitations of HDM*

The limitations of this method are essentially twofold. One is that individual pulses cannot be labeled as being either neutron or gamma pulses. There are ways in which this could

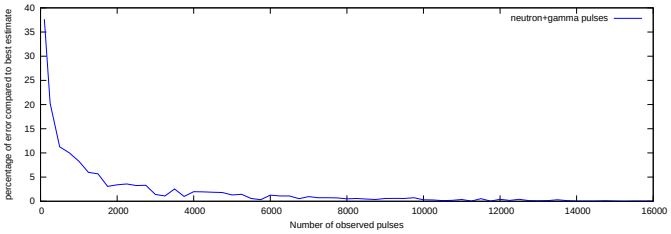


Fig. 15: The number of n+$\gamma$ pulses compared to the estimation of the percentage of neutrons measured from the n+$\gamma$ source.

be achieved, but they are beyond the scope of the work presented in this paper. Secondly, HDM only provides a lower bound on the percentage of neutrons in a source. That said, the estimates provided by HDM are very much in line with those provided by other, more sophisticated techniques, such as TOF. On the other hand, as we have pointed out above, the extreme simplicity of HDM will allow it to be implemented in Field-Programmable Gate Array (FPGA) inexpensive circuitry, which could ultimately mean the development of portable devices based on this technique.

## VI. Conclusion

This paper presents a very simple method, the Histogram-Difference Method (HDM), for calculating whether or not there is neutron emission from a given source and, in the affirmative, determines a lower bound on the percentage of neutron pulses from the source. The results produced by HDM correspond closely to the values found for neutron/gamma discrimination by other researchers using other techniques. We expect that this method will be further verified by a comparison to the results of other n/g discrimination methods, such as those relying on TOF and $He^3$ It is also possible that TOF from a pulsed neutron source could be used to produce a relatively clean neutron reference signal, but this is beyond the scope of the present paper.

This method does not rely on any particular encoding of pulses, but on a vector of extracted features obtained from the pulses. We have shown that HDM works for two independent representations derived from these extracted features. The representation-independence of HDM means that it would work with any number of other representations, such as, those based on Time-over-Threshold (ToT), rise-time, etc.

A further advantage of this method is that, even if some of the neutron pulses have representations that are identical to those of pure-$\gamma$ pulses, it is likely that the overall *distributions* of the representations for identical numbers n+$\gamma$ pulses and $\gamma$-only pulses will differ. And, based on this difference, we can derive a lower bound on the percentage of neutron pulses in the n+$\gamma$ source. It is crucial for HDM to work that there are exactly the same number of pulses from the $\gamma$-only source as from the n+$\gamma$ source.

We tested HDM using two different means of representing pulses, each of which bears very little resemblance to the other. We showed that the percentage of neutrons estimated by HDM for the set of (n+$\gamma$) pulses using both types of pulse representation was within $4\%$ of each other. As the HDM approach relies only on calculating differences in two histograms, the most computationally intensive part of the algorithm involves pulse pre-processing and feature extraction. However, because the $\gamma$-only reference histogram, $H_\gamma$, can be scaled to contain the same overall number of pulses as any $H_{n+\gamma}$ histogram, we can calculate $H_\gamma$ off-line and store it for later use. Practically, this means that calculating the difference between $H_\gamma$ and $H_{n+\gamma}$ will require only minimal computing resources and can be run on a small microcontroller (ARM), while the pulse pre-processing and feature extraction could easily be performed on any state-of-the-art FPGA. It is important to note that the HDM algorithm focuses on the calculation of the difference of two histograms built from features, but that the features per se are not important, as long as they provide an appropriate characterization of the pulses. One of the most common representations is to use pairs of values ($Q_{total}$, $Q_{tail}$), as we did. Another characterization is by means of D-values, which we also did. But any other vector of features (even more than 2D) could have been used. Selecting the best characterization of pulses is beyond the scope of this paper, but we would hope that researchers would suggest other means of characterizing pulses, including rise-times, time-over-threshold, etc. The point is that HDM is able to use of any kind of feature characterizing pulses, including rise-times, time-over-threshold, etc. and that these other, more detailed pulse representations will be given to HDM in the future to provide even better n/$\gamma$ discrimination.

## Acknowledgment

This work was cofunded by the French National Research Agency (ANR) and the French Prime Minister's Secrétariat Général la Défense et la Sécurité Nationale (SGDSN) – contract number ANR-14-CE28-0017.

## References

[1] S. N. Ahmed, "Gas-filled detectors," in *Physics and Engineering of Radiation Detection (Second Edition)*, second edition ed., S. N. Ahmed, Ed. Elsevier, 2015, pp. 157 – 231.

[2] D. A. Shea and D. Morgan, "The helium-3 shortage: Supply, demand, and options for congress," Congressional Research Service (USA), Tech. Rep., 2010. [Online]. Available: https://www.fas.org/sgp/crs/misc/R41419.pdf

[3] P. Peerani, A. Tomanin, S. Pozzi, J. Dolan, E. Miller, M. Flaska, M. Battaglieri, R. D. Vita, L. Ficini, G. Ottonello, G. Ricco, G. Dermody, and C. Giles, "Testing on novel neutron detectors as alternative to $^3$He for security applications," *Nuclear Instruments and Methods in Physics Research Section A: Accelerators, Spectrometers, Detectors and Associated Equipment*, vol. 696, pp. 110 – 120, 2012.

[4] C. W. E. van Eijk, "Inorganic scintillators for thermal neutron detection," *IEEE Transactions on Nuclear Science*, vol. 59, no. 5, pp. 2242–2247, Oct 2012.

[5] F. Pino, L. Stevanato, D. Cester, G. Nebbia, L. Sajo-Bohus, and G. Viesti, "Study of the thermal neutron detector ZnS(Ag)/LiF response using digital pulse processing," *Journal of Instrumentation*, vol. 10, no. 08, p. T08005, 2015.

[6] G. H. V. Bertrand, M. Hamel, S. Normand, and F. Sguerra, "Pulse shape discrimination between (fast or thermal) neutrons and gamma rays with plastic scintillators: State of the art," *Nuclear Instruments and Methods in Physics Research Section A: Accelerators, Spectrometers, Detectors and Associated Equipment*, vol. 776, pp. 114 – 128, 2015.

[7] M. Moszyński, G. Costa, G. Guillaume, B. Heusch, A. Huck, and S. Mouatassim, "Study of n-$gamma$ discrimination with NE213 and BC501A liquid scintillators of different size," *Nuclear Instruments and Methods in Physics Research Section A: Accelerators, Spectrometers, Detectors and Associated Equipment*, vol. 350, no. 1, pp. 226 – 234, 1994.

[8] C. W. van Eijk, "Neutron {PSDs} for the next generation of spallation neutron sources," *Nuclear Instruments and Methods in Physics Research Section A: Accelerators, Spectrometers, Detectors and Associated Equipment*, vol. 477, no. 13, pp. 383 – 390, 2002, 5th Int. Conf. on Position-Sensitive Detectors.

[9] A. Kaplan, M. Flaska, A. Enqvist, J. Dolan, and S. Pozzi, "EJ-309 pulse shape discrimination performance with a high gamma-ray-to-neutron ratio and low threshold," *Nuclear Instruments and Methods in Physics Research Section A: Accelerators, Spectrometers, Detectors and Associated Equipment*, vol. 729, pp. 463 – 468, 2013.

[10] S. D. Ambers, M. Flaska, and S. A. Pozzi, "A hybrid pulse shape discrimination technique with enhanced performance at neutron energies below 500 keV," in *2009 IEEE Nuclear Science Symposium Conference Record (NSS/MIC)*, Oct 2009, pp. 86–89.

[11] P. Blanc, M. Hamel, C. Dehé-Pittance, L. Rocha, R. B. Pansu, and S. Normand, "Neutron/gamma pulse shape discrimination in plastic scintillators: Preparation and characterization of various compositions," *Nuclear Instruments and Methods in Physics Research Section A: Accelerators, Spectrometers, Detectors and Associated Equipment*, vol. 750, pp. 1 – 11, 2014.

[12] C. C. Lawrence, M. M. Flaska, M. Ojaruega, A. Enqvist, S. D. Clarke, S. A. Pozzi, and F. D. Becchetti, "Time-of-flight measurement for energy-dependent intrinsic neutron detection efficiency," in *IEEE Nuclear Science Symposuim Medical Imaging Conference*, Oct 2010, pp. 110–113.

[13] A. Buffler, A. C. Comrie, F. D. Smit, and H. J. Wörtche, "A new compact neutron/gamma ray scintillation detector," *International Journal of Modern Physics Conference Series*, vol. 44, p. 1660228, Sep. 2016.

[14] S. Normand, V. Kondrasovs, G. Corre, J. M. Bourbotte, and A. Ferragut, "MA-NRBC: first successful attempt for neutron gamma discrimination in plastic scintillators," in *2011 2nd International Conference on Advancements in Nuclear Instrumentation, Measurement Methods and their Applications*, June 2011, pp. 1–4.

[15] S. D. Jastaniah and P. J. Sellin, "Digital pulse-shape algorithms for scintillation-based neutron detectors," *IEEE Transactions on Nuclear Science*, vol. 49, no. 4, pp. 1824–1828, Aug 2002.

[16] T. S. Sanderson, C. D. Scott, M. Flaska, J. K. Polack, and S. A. Pozzi, "Machine learning for digital pulse shape discrimination," in *2012 IEEE Nuclear Science Symposium and Medical Imaging Conference Record (NSS/MIC)*, Oct 2012, pp. 199–202.

[17] A. Buffler, A. C. Comrie, F. D. Smit, and H. J. Wrtche, "A new compact neutron/gamma ray scintillation detector," *International Journal of Modern Physics: Conference Series*, vol. 44, p. 1660228, 2016.

[18] X. Luo, V. Modamio, J. Nyberg, J. Valiente-Dobón, Q. Nishada, G. de Angelis, J. Agramunt, F. Egea, M. Erduran, S. Ertrk, G. de France, A. Gadea, V. González, T. Hüyük, G. Jaworski, M. Moszyński, A. D. Nitto, M. Palacz, P.-A. Sderstrm, E. Sanchis, A. Triossi, and R. Wadsworth, "Test of digital neutrongamma discrimination with four different photomultiplier tubes for the NEutron detector array (NEDA)," *Nuclear Instruments and Methods in Physics Research Section A: Accelerators, Spectrometers, Detectors and Associated Equipment*, vol. 767, pp. 83 – 91, 2014.

[19] R. M. Preston, J. E. Eberhardt, and J. R. Tickner, "Neutron-gamma pulse shape discrimination using organic scintillators with silicon photomultiplier readout," *IEEE Transactions on Nuclear Science*, vol. 61, no. 4, pp. 2410–2418, Aug 2014.

[20] J. B. Birks, "Scintillations from organic crystals: Specific fluorescence and relative response to different radiations," *Proceedings of the Physical Society. Section A*, vol. 64, no. 10, p. 874, 1951.

[21] R. Gehrke, R. Aryaeinejad, J. Hartwell, W. Yoon, E. Reber, and J. Davidson, "The -ray spectrum of 252cf and the information contained within it," *Nuclear Instruments and Methods in Physics Research Section B: Beam Interactions with Materials and Atoms*, vol. 213, pp. 10 – 21, 2004.

[22] K. Okamuto, "Neutron sources properties," in *Proceedings of The IAEA Consultants' Meeting on Neutron Sources*, IAEA. International Nuclear Data Comittee, 1980.

[23] A. Boulogne and A. Evans, "Californium-252 neutron sources for medical applications," *The International Journal of Applied Radiation and Isotopes*, vol. 20, no. 6, pp. 453 – 461, 1969.

[24] M. Flaska and S. Pozzi, "Identification of shielded neutron sources with the liquid scintillator bc-501a using a digital pulse shape discrimination method," *Nuclear Instruments and Methods in Physics Research Section A: Accelerators, Spectrometers, Detectors and Associated Equipment*, vol. 577, no. 3, pp. 654 – 663, 2007.

[25] M. Flaska and S. A. Pozzi, "Offline pulse-shape discrimination algorithms for neutron spectrum unfolding," in *2006 IEEE Nuclear Science Symposium Conference Record*, vol. 2, Oct 2006, pp. 752–758.

[26] R. R. Hansen, P. L. Reeder, A. J. Peurrung, and D. C. Stromswold, "Neutron-gamma discrimination in plastic scintillators," *IEEE Transactions on Nuclear Science*, vol. 47, no. 6, pp. 2024–2028, Dec 2000.

**Robert French** Robert French holds a Bachelor's and Master's Degree in mathematics and a Ph.D. from the University of Michigan (1992) in computer science, specializing in artificial intelligence and machine learning. His thesis co-advisors were John Holland and Douglas Hofstadter. He currently holds a senior research position (Research Director) in computational modeling at the French National Scientific Research Center (CNRS). His full CV can be found here: http://leadserv.u-bourgogne.fr/files/members/resumes/robert-m.-french.fr.pdf

**Mathieu Thevenin** Mathieu Thevenin obtained his B.S. (computer science, 2003) and Master's degrees (Computer science, Embedded systems and Instrumentation, 2006) from the University of Burgundy (France). His Ph.D. (University of Burgundy, 2009) focused on the design of a programmable, low-silicon footprint Digital Signal Processor (DSP) for real-time video enhancement. He currently holds a permanent expert-scientist position for the French Atomic Energy Commission (CEA). His research focuses on the design of programmable hardware architectures with a special emphasis on signal/video processing, neural networks, integration technology-independent reliability for digital circuits and, since 2011, CBRN-E applications. He has co-authored several patents and publications and is an senior IEEE member.

**Matthieu Hamel** Matthieu Hamel defended a PhD in organic chemistry from the University of Caen Basse-Normandie (France), in 2005. Since 2009, he holds a permanent position at the French Atomic Energy Commission (CEA) as an expert scientist. His main research focus is the development and preparation of luminescent polymers for CBRN-E detection.

**Eva Montbarbon** Eva MONTBARBON studied physics at the University of Strasbourg (France). After receiving her Master's Degree in engineering, specializing in ionizing radiation physics, detectors and instrumentation, she began a Ph.D. in 2014 at the French Atomic Energy Commission (CEA). Her research focuses primarily on discriminating fast neutrons from gamma rays.